Journal of Materials Chemistry A

Fabrication of Symmetric Supercapacitors Based on MOF-Derived Nanoporous Carbons

Journal:	*Journal of Materials Chemistry A*
Manuscript ID:	TA-ART-08-2014-004277.R1
Article Type:	Paper
Date Submitted by the Author:	19-Sep-2014
Complete List of Authors:	Salunkhe, Rahul; National Institute for Materials Science, World Premier International (WPI) Research Center for Materials Nanoarchitectonics (MANA) Kamachi, Yuichiro; National Institute for Materials Science, WPI Center for MANA Torad, Nagy; National Institute for Materials Science, World Premier International (WPI) Research Center for Materials Nanoarchitectonics (MANA) Hwang, Soo Min; University of Wollongong, Institute for Superconducting and Electronic Materials Sun, Ziqi; Univeristy of Wollongong, Institute for Superconducting and Electronic Materials, University of Wollongong Dou, Shi; University of Wollongong, University of Wollongong, Institute for Superconducting and Electronic Materials Kim, Jung Ho; Institute for Superconducting and Electronic Materials, Yamauchi, Yusuke; National Institute for Materials Science, WPI Center for MANA

Fabrication of Symmetric Supercapacitors Based on MOF-Derived Nanoporous Carbons

Rahul R. Salunkhe[1], Yuichiro Kamachi[1], Nagy L. Torad[1,2], Soo Min Hwang[3], Ziqi Sun[3], Shi Xue Dou[3], Jung Ho Kim[3], and Yusuke Yamauchi*[1,2]

1 *World Premier International (WPI) Research Center for Materials Nanoarchitectonics (MANA), National Institute for Materials Science (NIMS), 1-1 Namiki, Tsukuba, Ibaraki 305-0044, Japan.*

2 *Faculty of Science and Engineering, Waseda University, 3-4-1 Okubo, Shinjuku, Tokyo 169-8555, Japan.*

3 *Institute for Superconducting and Electronic Materials, University of Wollongong, North Wollongong, New South Wales 2500, Australia.*

Corresponding author: Yamauchi.Yusuke@nims.go.jp

Homepage: http://www.yamauchi-labo.com

Abstract

Nanoporous carbon (NPC) materials with high specific surface area have attracted considerable attention for electrochemical energy storage applications. In the present work, we have designed novel symmetric supercapacitors based on NPC by direct carbonization of Zn-based metal organic frameworks (MOFs) without using additional precursor. By controlling the reaction conditions in the present study, we synthesize NPC with two different particle sizes. The effects of particle size and of mass loadings on supercapacitor performance have been carefully evaluated. Our NPC materials exhibit excellent electrochemical performance with a maximal specific capacitance of 251 $F \cdot g^{-1}$ in 1 M H_2SO_4 electrolyte. The symmetric supercapacitor studies show that these efficient electrodes have good capacitance, high stability, and good rate capability.

Keywords: porous material; nanoporous carbon; metal-organic framework; electrical double layer capacitor; symmetric supercapacitor

1. Introduction

Nanoporous carbon (NPC) materials have attracted considerable attention because of their extensive applications, such as in adsorbents, catalyst supports, electrode materials for electric double layer capacitors (EDLCs), Li-ion battery, and fuel cells [1-5]. Highly porous carbons can be prepared via a variety of methods, including activation (physical or chemical) of carbon, carbonization of polymer aerogels, and templating methods using zeolite and mesoporous silica [6-10]. Each approach has its own advantages for the formation of carbons with controlled pore texture and/or improved surface area, which are of great importance and considered to be the key factors in optimizing the performance in most applications.

Recently, porous metal-organic frameworks (MOFs), which are emerging as a new class of crystalline porous materials with multiple functionalities, have been the subject of great interest [11-13]. MOFs have been demonstrated as precursors to NPC materials, ever since the first report by Xu *et al.* [14-20]. MOF-derived NPCs have emerged as a novel type of porous material that combines well-defined shape and high surface area, which makes them good candidates for energy storage applications. The design of a simple and reliable method for the rational synthesis of NPC still remains a big challenge and may be of great interest in the field of energy storage applications.

Electrochemical capacitors (supercapacitors) consisting of two closely spaced layers with opposing charges have been widely used to power up electrical vehicles, consumer electronics, and military devices [21]. Electrochemical supercapacitors bridge the gap between batteries, which offer high energy densities but are slow, and conventional capacitors, which are fast but have low energy density [22-24]. For some power applications, however, a major limitation of supercapacitors is that they have unsatisfactory energy density (less than 10 $W{\cdot}h{\cdot}kg^{-1}$) compared to lead acid batteries (30-40 $W{\cdot}h{\cdot}kg^{-1}$) and lithium ion cells (160 $W{\cdot}h{\cdot}kg^{-1}$).[25] The advantages of electrical double layer capacitors (EDLCs) over other power source technology could become even greater if their electrodes were properly optimized with respect to pore size [26]. In breakthrough research, Chmiola *et al.* found

an anomalous increase in capacitance for pore size of less than 1 nm in carbide derived carbon [27]. From a literature survey, it is found that this anomalous behavior is not so unique to organic electrolyte or carbide-derived carbon [28]. Thus, research efforts have been, on the one hand, focusing on increasing the specific surface area of carbon-based electrodes, and on the other hand, looking for an appropriate pore structure to match with an electrolyte for improving the performance of EDLCs.

Very recently, we have proposed a direct carbonization of ZIF-8 to prepare NPCs for sensing and biomedical applications.[29-31] The obtained NPC particles possess a high specific surface area of 1523 $m^2 \cdot g^{-1}$ with an average pore diameter of ~1 nm, which makes them attractive materials for supercapacitor application. In the present work, we have designed novel symmetric supercapacitors based on ZIF-derived NPCs. This work can provide a rapid platform towards synthesis of promising carbons for supercapacitor application (**Figure 1-1**). As described in the experimental section, ZIF-8 is directly carbonized at 800 °C under nitrogen flow in a one-pot approach without any complicated steps or addition of any carbon source. After the carbonization, the obtained black powder is washed thoroughly with an acid solution to remove the existing zinc nanoparticles. The effects of particle size and of the mass loading on supercapacitor performance have been carefully investigated. Interestingly, our NPC sample shows excellent supercapacitor performance with a maximal specific capacitance of 251 $F \cdot g^{-1}$ at a scan rate of 5 $mV \cdot s^{-1}$. Interestingly, the symmetric supercapacitor studies for this material show a high energy density of 10.86 $W \cdot h \cdot kg^{-1}$ and an acceptable power density of 225 $W \cdot kg^{-1}$.

2. Experimental

Chemicals: 2-methylimidazole (MIM, purity 99%) and $Zn(CH_3COO)_2$ (purity 97%) were purchased from Sigma-Aldrich Chemical Co. Polyvinylpyrrolidone (PVP, K30), hydrochloric acid solution, and methanol were obtained from Nacalai Tesque Reagent Co. All raw chemicals were used without further purification.

Synthesis of large-sized ZIF-8 crystals (Average particle diameter ≥ 1 μm) and small-sized ZIF-8 crystals (Average diameter ~300 nm): According to our previous report [29-30], two types of ZIF-8 crystals were prepared by different approaches. For large-sized ZIF-8 crystals, $Zn(CH_3COO)_2$ and PVP were dissolved in methanol to form a solution. 2-methylimidazole was dissolved in methanol to generate another clear solution. Then, the above two solutions were mixed together and stirred for 5 min. The mixed solution was aged at room temperature for 24 h. After the white powders were precipitated, they were washed very carefully with methanol and dried. For small-sized ZIF-8 crystals, dried powders of both $Zn(CH_3COO)_2$ and 2-methylimidazole were directly mixed. Then, the mixed powder was dissolved in methanol. The solution was stirred for 5 min. Then, the solution was aged at room temperature for 24 hours. After the white powders were precipitated, they were washed very carefully with methanol and dried.

Carbonization of ZIF-8 samples: The obtained ZIF-8 particles were directly carbonized under flowing nitrogen gas at 800 °C. The temperatures inside the furnace were gradually increased from room temperature to the target temperatures with a heating rate of 5 $°C \cdot min^{-1}$. After the target temperature was reached, the powders were annealed for 5 h and then cooled down to room temperature. The obtained particles were collected and carefully washed with HF aqueous solution (10 %) to remove the Zn nanoparticles. The sample was stirred in the HF solution for 24 h and then collected. The sample was washed 4 times in distilled water and then dried under vacuum conditions for 24 h at 60 °C.

Materials characterization: The surface morphology and nanostructure were investigated using scanning electron microscopy (SEM, Hitachi S-4800) and transmission electron microscopy (TEM, JEM-2100F, 200 kV). The crystalline structures of the samples were characterized using a powder X-ray diffraction (Rigaku 2500) system equipped with Cu Kα radiation (λ = 0.15406 nm). Nitrogen adsorption-desorption isotherms were collected on a Quantachrome Autosorb Automated Gas Sorption System at 77 K.

Electrochemical measurements: The electrochemical measurements were conducted on a three-electrode system using Pt as the counter electrode and Ag/AgCl as the reference electrode in 1 M H_2SO_4 solution. Graphite substrate coated with ZIF-8 carbon (1 mg) was used as the working electrode. (The graphite substrate serves as the current collector.) The graphite substrates were firstly polished under flowing water using a fine polisher. Then, they were washed with deionized water, etched in a 0.1 M HCl solution at room temperature for 10 min, and finally washed with deionized water in an ultrasonic bath for 30 min. The mass of the electrodes was measured using an ultra-microbalance (METTLER TOLEDO). The carbon sample was mixed with poly(vinylidine difluoride) (PVDF, 20%) in N-methyl 2-pyrrolidinone (NMP) solvent. The resulting slurry was homogenized by ultrasonication and coated onto a graphite substrate, which was followed by drying at 80 °C for 2 h in a vacuum oven. Cyclic voltammograms (CV curves) were obtained using an electrochemical workstation (CHI 660E CH Instruments, USA) in the scan range of 0 to 0.6 V. For every experiment, the typical area under consideration was 1 × 1 cm^2. The specific capacitance value was calculated from the CV curve using the following Equation (1),

$$C = \frac{1}{ms(V_f - V_i)} \int_{V_i}^{V_f} I(V)dv \qquad (1)$$

where '*m*' is the mass of active electrode material, '*s*' is the potential scan rate, V_f and V_i are the integration limits of the voltammetric curve, and *I(V)* denotes the current response, respectively.

Furthermore, the electrochemical properties of the symmetric supercapacitor were investigated by CV and galvanostatic charge-discharge measurements. For the charge-discharge measurements, two-electrode symmetric cells were employed, each with a positive and a negative electrode consisting of NPC samples with a similar charge capacity. The charge-discharge current density based on the mass loading of the electrodes was varied from 0.5 $A \cdot g^{-1}$ to 10 $A \cdot g^{-1}$ to evaluate the specific energy and specific power of the device. The specific capacitance (*C*, $F \cdot g^{-1}$), specific energy (*SE*, $W \cdot h \cdot kg^{-1}$), and specific power (*SP*, $kW \cdot kg^{-1}$) were calculated from the chronopotentiometric curves using the following Equations (2-4), respectively.

$$C = \frac{I \times \Delta t}{m \times \Delta V} \quad (2)$$

$$SE = \frac{\frac{1}{2} C V^2}{3.6} \quad (3)$$

$$SP = \frac{3600 \times SE}{t} \quad (4)$$

Where *I* is the charge/discharge current at a discharge time *t* (s), ΔV is the potential window, and '*m*' is the mass of the electrode.

3. Results and discussion

Figure 2(a) is an SEM image of the large-sized NPC. It can be observed that these particles have good uniformity with average particle size of ~1 μm. **Figure 2(b)** is a highly magnified SEM image of the NPC which shows highly-symmetric geometry, with each particle polyhedral in shape with very sharp edges. The SEM and TEM images [**Figure 2(b-c)**] demonstrate that the obtained carbons have the original morphology of ZIF-8. **Figure S1** in the Supporting Information contains an SEM image of the small-sized NPC (~ 300 nm). From the SEM image, it is clear that these particles also have polyhedral shapes. Thus, we can easily control the size of particles by this method by changing the reaction conditions.[29-30] These NPC samples were examined by powder X-ray diffraction [**Figure 2(d)**]. The obvious peaks observed at around 25° belong to a typical (002) interlayer peak of graphite-type carbon. The chemical compositions of the NPC samples were analyzed by energy-dispersive X-ray spectroscopy (EDS) elemental mapping [**Figure S2 (a-c)**], where the elements carbon and nitrogen were found to be incorporated within the NPC. CHN analysis was carried out to determine the exact nitrogen content in the present samples. It was found that the content of nitrogen in the present samples is almost 15 %.

The NPC was carefully evaluated by nitrogen gas adsorption-desorption isotherms [**Figure S2(d)**]. These particles show type I isotherms, which is typical of microporous materials. From nonlinear density functional theory (NLDFT) analysis of the nitrogen adsorption isotherms [**Figure S2(d)**], it was found that the average pore size was around 1 nm. Benefiting from the microporous structure, the surface area of these NPC particles was extremely high (1523 $m^2 \cdot g^{-1}$). This large specific surface area includes a relatively small contribution from the surface area of the particles and a major contribution from the nanopores inside the particles.

The CV experiments were employed to characterize the capacitive performances of the NPC (**Figure 3**). Graphite substrates coated with NPC samples were used as the working electrode for electrochemical analysis. CV experiments were conducted by using the three-electrode system in a 1 M

H_2SO_4 solution. The reference electrode and the counter electrode were Ag/AgCl and platinum, respectively. Firstly, comparative electrochemical studies were carried out on the small-sized and large-sized NPC. For both, the supercapacitor electrode exhibited stable operation in the potential range of 0 to 0.9 V. The capacitance value obtained from the CV curves (using **Equation 1**) for the small-sized NPC (**Figure S3**) was about 125 $F \cdot g^{-1}$ at 5 $mV \cdot s^{-1}$ scan rate, which was much lower than that of the large-size NPC, for which the capacitance value was 251 $F \cdot g^{-1}$ at the same scan rate (**Figure 3**). This can be explained as, in the case of the small-sized NPC, particle aggregation were observed in the suspension, due to the strong interaction between the fine particles, which causes them to become bound to each other (close-fitting). This fact limits the ability of the electrolyte to penetrate inside to deep pore surfaces, resulting in a decrease in capacitance.

Figure 3(a) shows the CVs of large-sized NPC in 1 M H_2SO_4 electrolyte at various scan rates ranging from 5 to 200 $mV \cdot s^{-1}$. The obtained CV curve is almost rectangular in shape, which is ideal for EDLC type capacitors. Even at the high scan rates of 500, 700, and 1000 $mV \cdot s^{-1}$, the CVs show almost rectangular behavior, indicating good transport properties at higher scan rates (**Figure S4**). This result indicates high capacitance retention (50 %), even at the very high scan rate of 1000 $mV \cdot s^{-1}$, which is much higher than in previous reports on MOF-derived NPC supercapacitors [19, 31]. It is well known that the presence of some chemical functionalities, containing heteroatoms (nitrogen) gives carbon materials an acid/base character and thus enhances the capacitance by the same pseudocapacitive effect [32]. It has been reported that the presence of nitrogen contacting groups leads to improved electrical conductivity through carbon material, resulted into superior capacitance retention during fast charge-discharge process [33]. Thus, the significant amount of nitrogen in our sample (~15 %, as confirmed from CHN analysis) helps to retain the ideal rectangular CV shape, even at very high rates, which improves the capacitance retention of the sample.

In order to understand the details of carbon and nitrogen content in the large-sized NPC, we discussed the XPS data very carefully, according to our previous literature [30]. The C 1s spectrum can

be fitted into six peaks [**Figure S5(a)**]. The C_1 peak at 284.3 is assigned to a graphitic carbon structure (sp^2 C=C) [34], while the C_2 peak at 284.9 eV is quite close to the binding energy of sp^3 C-C [35]. The C_3 peak at 285.9 eV is assigned to C atoms directly bonded to oxygen in hydroxyl configuration (C-OH) [35]. The C_4 peak at 287.0 eV is ascribed to sp^3 C-N [36]. The small peaks centered around 288.9 and 290.9 eV (C_5 and C_6) are related to carboxy groups and the π-π* electronic transition, respectively [37]. The enlarged N 1s spectrum can be fitted into four peaks [**Figure S5(b)**]. The N_1 peak at 397.9 eV corresponds to a pyridinic nitrogen, that is, one nitrogen atom bonded to two C atoms in a hexagonal ring [38]. The N_2 peak at 399.5 eV can be assigned to sp^2 nitrogen atoms bonded to carbon atoms [39]. The N_3 peak centered at 400.4 eV represents a pyrrolic nitrogen [40]. The N_4 peak at the highest binding energy (403.5 eV) is undoubtedly attributed to molecular N_2 [41]. It is well known that the incorporation of nitrogen atoms into carbon creates structural defects. The carbon atoms at the edge sites are highly reactive with physically adsorbed oxygen and form oxygen-containing groups when exposed to air [42]. From the XPS analysis, the proportions of carbon, nitrogen, and oxygen are calculated to be 81.0 %, 13.6 %, and 4.0 %, respectively. These values almost coincide with the CHN data.

As seen in **Figure 3(b)**, the specific capacitance values calculated from the CVs were 252, 208, 195, 186, 180, 175, 166, 159, 133, 129, and 125 $F \cdot g^{-1}$ at the different scan rates of 5, 20, 40, 60, 80, 100, 150, 200, 500, 700, and 1000 $mV \cdot s^{-1}$, respectively. The obvious advantage of the pore structure, where solvated ions interact between pore walls, is responsible for the major contribution to the capacitance value. To the best of our knowledge, the present capacitance values are very high among all the NPC values measured in an aqueous electrolyte using a three electrode arrangement. The decrease in the capacitance at higher scan rates indicates that the electrolyte gets a shorter diffusion time inside the pores. Furthermore, to study the effects of different weight loadings on capacitance performance, we varied the weight of active electrode material and tested the capacitance performance (**Figure 4**). The obtained capacitance values (retention in capacitance after 200 $mV \cdot s^{-1}$) were 208 $F \cdot g^{-1}$

(63 %), 195 $F \cdot g^{-1}$ (74 %), and 124 $F \cdot g^{-1}$ (75 %) at different weight loadings of 1.0, 1.5, and 2.0 $mg \cdot cm^{-1}$, respectively. The results show that the capacitance values decreased with increased weight loading, while the retention in capacitance is slightly improved at higher weight loadings. At higher weight loadings, the whole carbon surface is not accessible from the outside, so that the dead area in the inner part of the sample causes the decrease in the capacitance value.

Towards practical use, we fabricated a symmetric supercapacitor cell by using the NPCs as electrode material (**Figure 1-2**). For the charge/discharge measurements on the symmetric cell, we employed both a positive electrode and a negative electrode of ZIF-8 derived NPC with similar charge capacity separated by electrolyte without use of any separator. To obtain stable symmetric cell operated in wide potential range, it is necessary to balance the charge (Q) that is stored on both positive and negative electrodes. Based on the open-circuit potentials of the positive and negative electrodes, a similar charge capacity (but not capacitance) was adjusted on both the positive and negative electrodes when the upper and lower potential limits of the positive and negative electrodes were set. **Figure 5(a)** shows the CV curves of the symmetric supercapacitor for various scan rates at various sweep rates from 5 to 200 $mV \cdot s^{-1}$ in the potential range of 0.0 V to 0.9 V. The CV curves show a typical rectangular shape from 0 to 0.9 V. The CV shape is mirror-symmetric, even at high scan rate, indicating the high reversibility of the sample. Above this potential cut-off of 0.9 V, the CV curve shows a distortion and a slight hump at around 1.0 V. This indicates that some irreversible reactions occur when the potential window is higher than 0.9 V. Thus, the optimum working potential window for this symmetric supercapacitor is set from 0 to 0.9 V.

To further evaluate the electrochemical performance of the symmetric cell, galvanostatic charge/discharge tests were performed at various current densities, as shown in **Figure 5(b)**. The charge/discharge current density, based on the total mass loading of NPC, was varied from 0.5 to 5 $A \cdot g^{-1}$ to evaluate the specific energy and power of the device. All of the curves showed typical linear discharge curves, indicating well-balanced charge storage. The symmetric device showed high

capacitance value of 98 $F \cdot g^{-1}$ (at 0.5 $A \cdot g^{-1}$). Even at 10 times higher current density (at 5 $A \cdot g^{-1}$), it still showed high capacitance value is 62 $F \cdot g^{-1}$, indicating good rate capability (**Figure 5(c)**). This also suggests the ability of the system to deliver high power.

To evaluate the supercapacitor performance of our symmetric cell, our values of specific energy and specific power were plotted in a Ragone plot, as shown in **Figure 5(d)**. This device showed a high specific energy of 10.86 $W \cdot h \cdot kg^{-1}$ at a specific power of 225 $W \cdot kg^{-1}$, at a current density of 0.5 $A \cdot g^{-1}$. At 5 $A \cdot g^{-1}$, the specific power increases to 2281 $W \cdot kg^{-1}$, maintaining the specific energy of 6.97 $W \cdot h \cdot kg^{-1}$. A direct comparison of our symmetric capacitor performance with previous reports [43-46] in the literature is summarized in **Table 1**. This type of electrode is useful where moderate energy density and moderate power density are required. To further demonstrate the advantages of NPC for supercapacitor application, life cycle test was carried out using galvanostatic charge-discharge studies at a current density of 7.5 $A \cdot g^{-1}$ (capacitance value at this current density was 41 $F \cdot g^{-1}$) up to 2,000 cycles [**Figure 6(a)**]. More interestingly, these electrodes exhibited stable performance up to 2000 cycles with a negligible loss of only 8 %. The arbitrarily chosen charge-discharge cycles also show the good stability performance of the electrode [**Figure 6(b)**]. These results highlight the merits of our symmetric capacitor to meet the requirements of high stability and good rate capability. These interesting characteristics of our symmetric supercapacitor cell, such as good specific energy/specific power and high cycling performance, which forms a new era for researchers to explore high-performance electrochemical energy storage devices based on MOF derived nanoporous materials.

4. Conclusion

We have designed novel symmetric supercapacitors based on NPC by direct carbonization of ZIF-8. The NPC used in this study showed a very high surface area of 1,523 $m^2 \cdot g^{-1}$, with an average pore diameter of ~1 nm, and demonstrated good potential as a capacitive electrode. The NPC showed a maximum capacitance of 251 $F \cdot g^{-1}$ at a scan rate of 5 $mV \cdot s^{-1}$. The symmetric supercapacitor based on NPC featured a specific energy of 10.86 $W \cdot h \cdot kg^{-1}$, with an acceptable specific power of 225 $W \cdot kg^{-1}$. These results highlight the merits of ZIF-8 derived NPC to meet the requirements of both long cycle life and good rate capability. Thus, this simple and low cost method demonstrated in the present work could be extended to the fabrication of other NPC materials with optimized pore architectures for next-generation energy storage applications. Our work can provide an easy platform for progress towards synthesis of promising carbons for supercapacitor applications.

References

[1] R. Ryoo, S. H. Joo, M. Kruk, M. Jaroniec, Adv. Mater. 13 (2001) 677.

[2] J. Lee, J. Kim, T. Hyeon, Adv. Mater. 18 (2006) 2073.

[3] J. Tang, J. Liu, N. L. Torad, T. Kimura, Y. Yamauchi, Nano Today 9 (2014) 305.

[4] P. Simon, Y. Gogotsi, Acc. Chem. Res. 46 (2013) 1094.

[5] Y. Tao, M. Endo, M. Inagaki, K. Kaneko, J. Mater. Chem. 21 (2011) 313.

[6] B. Hu, K. Wang, L. Wu, S. H. Yu, M. Antonietti, M. M. Titirici, Adv. Mater. 22 (2010) 813.

[7] X. Ji, K. T. Lee, L. F. Nazar, Nature Mater. 8 (2009) 500.

[8] S. H. Joo, S. J. Choi, I. Oh, J. Kwak, Z. Liu, O. Terasaki, R. Ryoo, Nature 412 (2001) 169.

[9] H. Nishihara, P. X. Hou, L. X. Li, M. Ito, M. Uchiyama, T. Kaburagi, A. Ikura, J. Katamura, T. Kawarada, K. Mizuuchi, T. Kyotani, J. Phys. Chem. C 113 (2009) 3189.

[10] J. Liu, T. Y. Yang, D. W. Wang, G. Q. Lu, D. Y. Zhao, S. Z. Qiao, Nature Commun. 4 (2013) 2798.

[11] H. Li, M. Eddaoudi, M. O'Keeffe, O. Yaghi, Nature 402 (1999) 276.

[12] M. Kondo, S. Furukawa, K. Hirai, T. Tsuruoka, J. Reboul, H. Uehara, S. Diring, Y. Sakata, O. Sakata, S. Kitagawa, J. Am. Chem. Soc. 136 (2014) 4938.

[13] K. S. Park, Z. Ni, A. P. Cote, J. Y. Choi, R. Huang, F. J. U. Romo, H. K. Chae, M. O'Keeffe, O. M. Yaghi, PNAS 103 (2006) 10186.

[14] B. Liu, H. Shioyama, T. Akita, Q. Xu, J. Am. Chem. Soc. 130 (2008) 5390.

[15] H. L. Jiang, B. Liu, Y. Q. Lan, K. Kuratani, T. Akita, H. Shioyama, F. Zong, Q. Xu, J. Am. Chem. Soc. 133 (2011) 11854.

[16] B. Liu, H. Shioyama, H. Jiang, X. Zhang, Q. Xu, Carbon 48 (2010) 456.

[17] M. Hu, J. Reboul, S. Furukawa, N. L. Torad, Q. Ji, P. Srinivasu, K. Ariga, S. Kitagawa and Y. Yamauchi, J. Am. Chem. Soc. 134 (2012) 2864.

[18] W. Chaikittisilp, K. Ariga, Y. Yamauchi, J. Mater. Chem. A 1 (2013) 14.

[19] N. L. Torad, R. R. Salunkhe, Y. Li, H. Hamoudi, M. Imura, Y. Sakka, C. C. Hu, Y. Yamauchi, Chem. Eur. J. 20 (2014) 7895.

[20] A. J. Amali, J. K. Sun, Q. Xu, Chem. Commun. 50 (2014) 1519.

[21] G. Wang, L. Zhang, J. Zhang Chem. Soc. Rev. 41 (2012) 797.

[22] C. C. Hu, W. C. Chen, K. H. Chang, J. Electrochem. Soc. 151 (2004) A281.

[23] H. Y. Hsu, K. H. Chang, R. R. Salunkhe, C. T. Hsu, C. C. Hu, Electrochim. Acta 94 (2013) 104.

[24] S. Makino, Y. Yamauchi, W. Sugimoto, J. Power Sources 227 (2013) 153.

[25] L. L. Zhang, X. S. Zhao, Chem. Soc. Rev. 38 (2009) 2520.

[26] S. Kondrat, C. R. Pérez, V. Presser, Y. Gogotsi, A. A. Kornyshev, Energy Environ. Sci., 5 (2012) 6474.

[27] J. Chmiola, G. Yushin, Y. Gogotsi, C. Portet, P. Simon, P. L. Taberna, Science 313 (2006) 1760.

[28] J. Huang, B. G. Sumpter, V. Meunier, Chem. Eur. J. 14 (2008) 6614.

[29] N. L. Torad, M. Hu, Y. Kamachi, K. Takai, M. Imura, M. Naito, Y. Yamauchi, Chem. Commun. 49 (2013) 2521.

[30] N. L. Torad, Y. Li, S. Ishihara, K. Ariga, Y. Kamachi, H. Y. Lian, H. Hamoudi, Y. Sakka, W. Chaikittisilp, K. C. W. Wu, Y. Yamauchi, Chem. Lett. 43 (2014) 717.

[31] W. Chaikittisilp, M. Hu, H. Wang, H. S. Huang, T. Fujita, K. C. W. Wu, L. C. Chen, Y. Yamauchi, K. Ariga, Chem. Commun. 48 (2012) 7259.

[32] L. Zhao, L. Z. Fan, M. Q. Zhou, H. Guan, S. Qiao, M. Antonietti, M. M. Titirici, Adv. Mater. 22 (2010) 5202.

[33] D. H. Jurcakova, M. Seredych, G. Q. Lu, T. J. Bandosz, Adv. Funct. Mater. 19 (2009) 438.

[34] Y. Xia, R. Mokaya, Chem. Mater. 17 (2005) 1553.

[35] A. Ganguly, S. Sharma, P. Papakonstantinou, J. Hamilton, J. Phys. Chem. C 115 (2011) 17009.

[36] B. Angleraud, N. Mubumbila, P. Y. Tessier, V. Fernandez, G. Turban, Diamond Relat. Mater. 10 (2001) 1142.

[37] K. Yang, M. Gu, Y. Guo, X. Pan, G. Mu, Carbon 47 (2009) 1723.

[38] J. R. Pels, F. Kapteijn, J. A. Moulijn, Q. Zhu, K. M. Thomas, Carbon 33 (1995) 1641.

[39] J. Tang, T. Wang, X. Pan, X. Sun, X. Fan, Y. Guo, H. Xue, J. He, J. Phys. Chem. C 117 (2013) 16896.

[40] Y. Shao, S. Zhang, M. H. Engelhard, G. Li, G. Shao, Y. Wang, J. Liu, I. A. Aksay, Y. Lin, J. Mater. Chem. 20 (2010) 7491.

[41] A. Lushington, J. Liu, Y. Tang, R. Li, X. Sun, J. Vac. Sci. Technol. A 32 (2014) 01A124.

[42] T. I. T. Okpalugo, P. Papakonstantinou, H. Murphy, J. McLaughlin, N. M. D. Brown, Carbon 43 (2005) 153.

[43] X. He, R. Li, J. Qiu, K. Xie, P. Ling, M. Yu, X. Zhang, M. Zheng, Carbon 50 (2012) 4911.

[44] Q. Wang, J. Yan, T. Wei, J. Feng, Y. Ren, Z. Fan, M. Zhang, X. Jing, Carbon 60 (2013) 481.

[45] M.P. Bichat, E. R. Piñero, F. Béguin, Carbon 48 (2010) 4351.

[46] Q. Wang, J. Yan, Y. Wang, G. Ning, Z. Fan, T. Wei, J. Cheng, M. Zhang, X. Jing, Carbon 52 (2013) 209.

Table 1 Comparison of our symmetric supercapacitor data with reported carbon-based symmetric supercapacitors using different aqueous electrolytes.

No.	System	Electrolyte	Current density ($A \cdot g^{-1}$)	Scan rate ($mV \cdot s^{-1}$)	Specific energy ($Wh \cdot kg^{-1}$)	Specific power ($W \cdot kg^{-1}$)	Ref.
1	**NPC**	**1 M H_2SO_4**	**0.5**	**-**	**10.86**	**225**	**Present work**
2	Mesoporous carbon	6 M KOH	0.05	-	8.42	-	[43]
3	Mesoporous carbon	1 M Na_2SO_4	-	5	9.6	119.4	[44]
4	Seaweed carbon	H_2SO_4	0.2	-	12.6	-	[45]
		KOH		-	4.4	-	
		Na_2SO_4		-	10.7	-	
5	Carbon spheres + CNTs	6 M KOH	-	5	11.3	11800	[46]

Figure 1

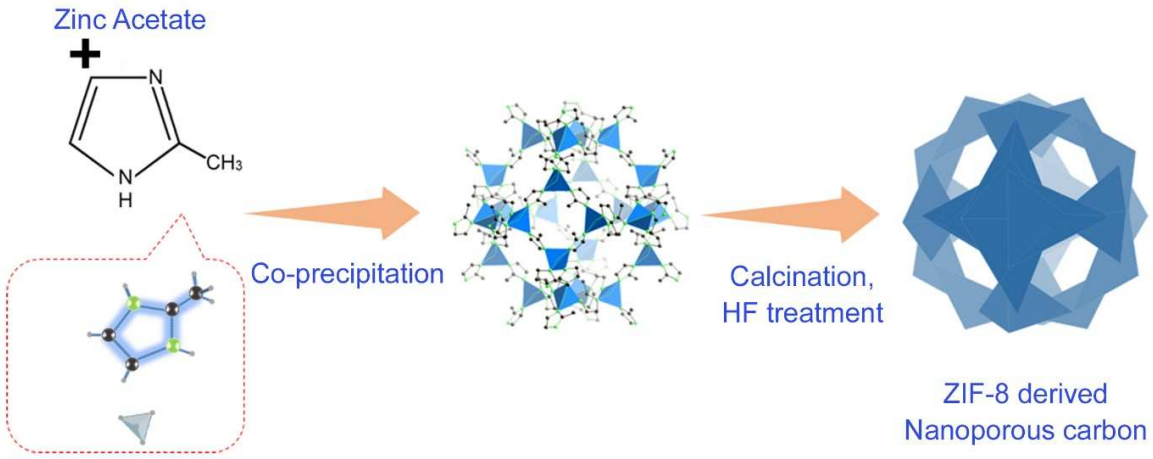

Figure 1-1 | Schematic illustration of synthesis of NPC materials derived from MOFs.

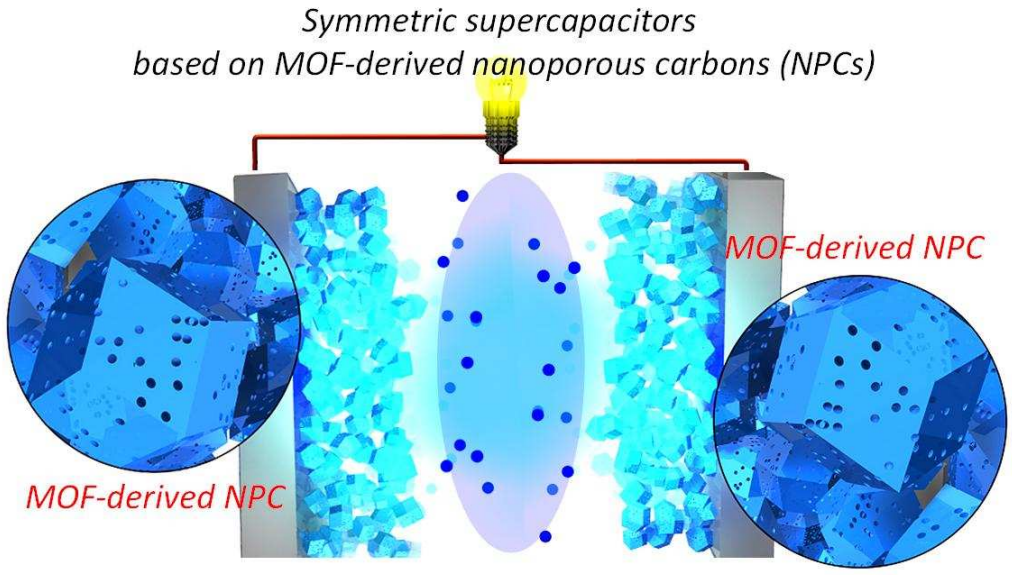

Figure 1-2 | Illustration of symmetric supercapacitor based on MOF-derived nanoporous carbons (NPCs). The symmetric supercapacitor cell is fabricated by the two electrodes of MOF-derived NPC with similar charge capacity separated by electrolyte without use of any separator.

Figure 2

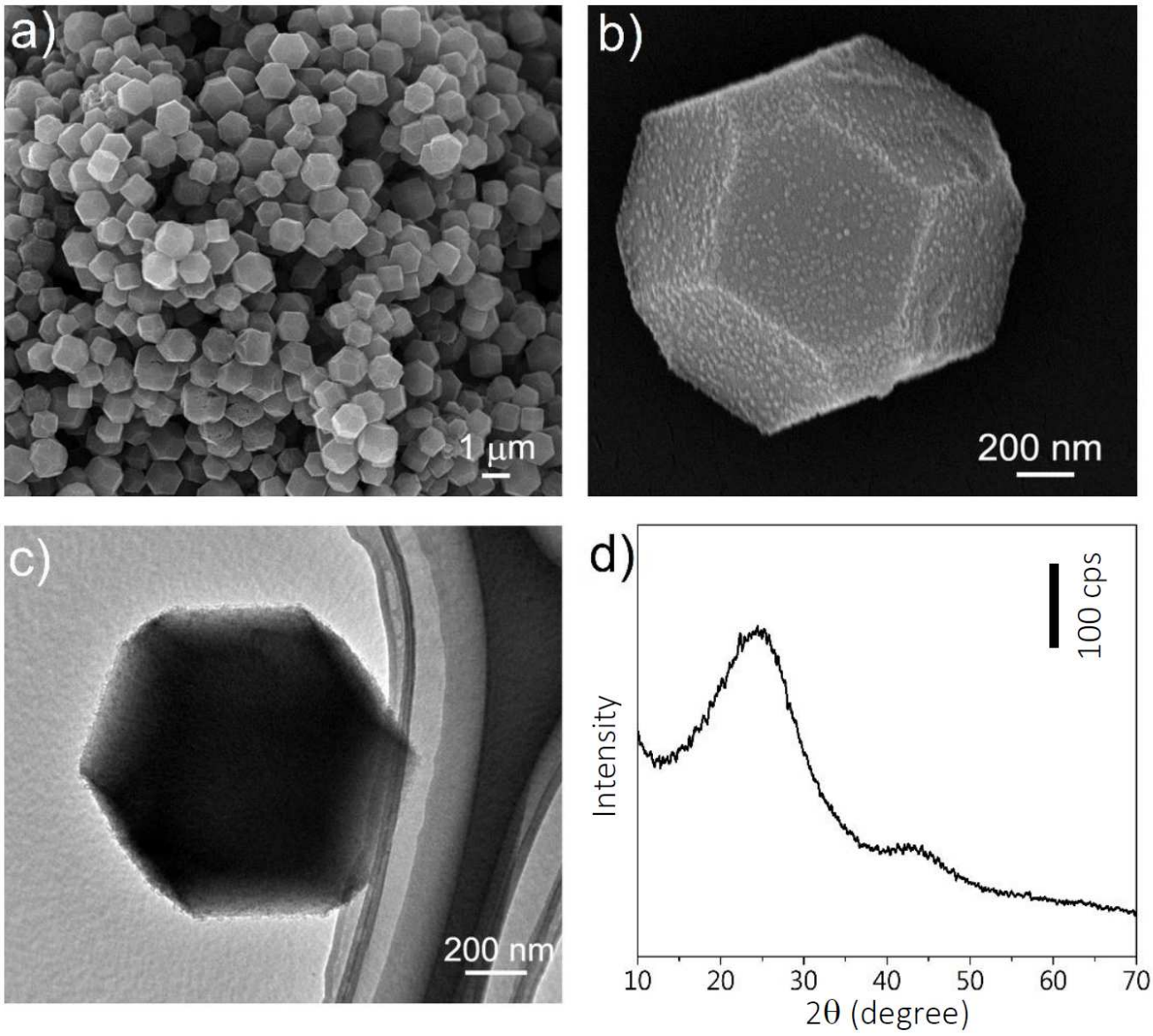

Figure 2 | (a-b) SEM images of large-sized NPC at different magnifications, (c) TEM image of one NPC particle, and (d) wide-angle XRD pattern of large-sized NPC.

Figure 3

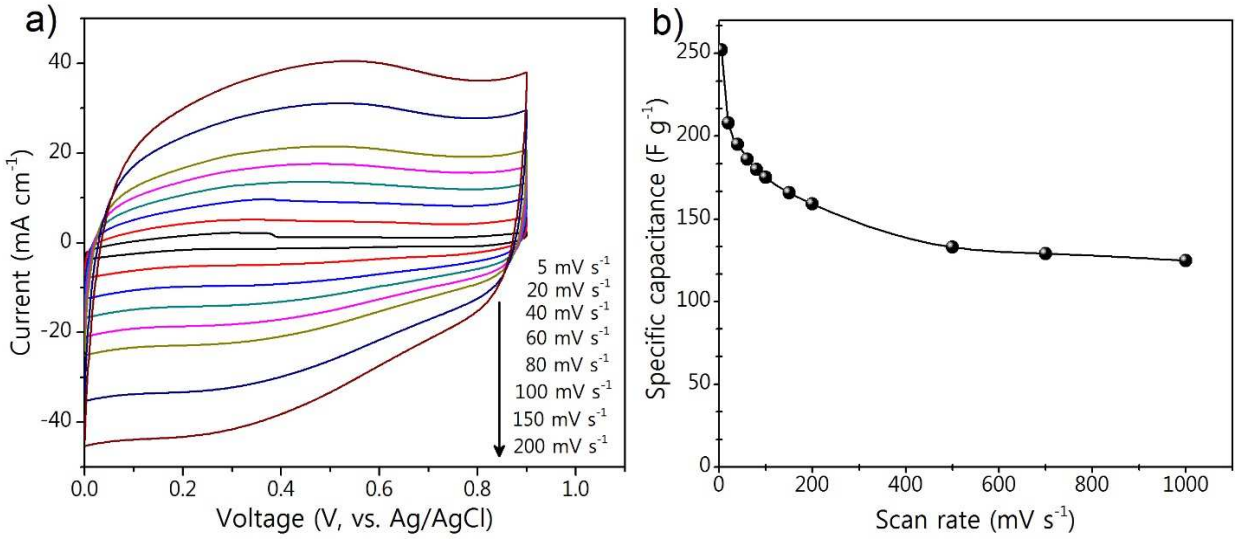

Figure 3 | (a) CV curves of large-sized NPC at various scan rates from 5 to 200 mV·s^{-1} and (b) variation of the specific capacitance with the applied scan rate.

Figure 4

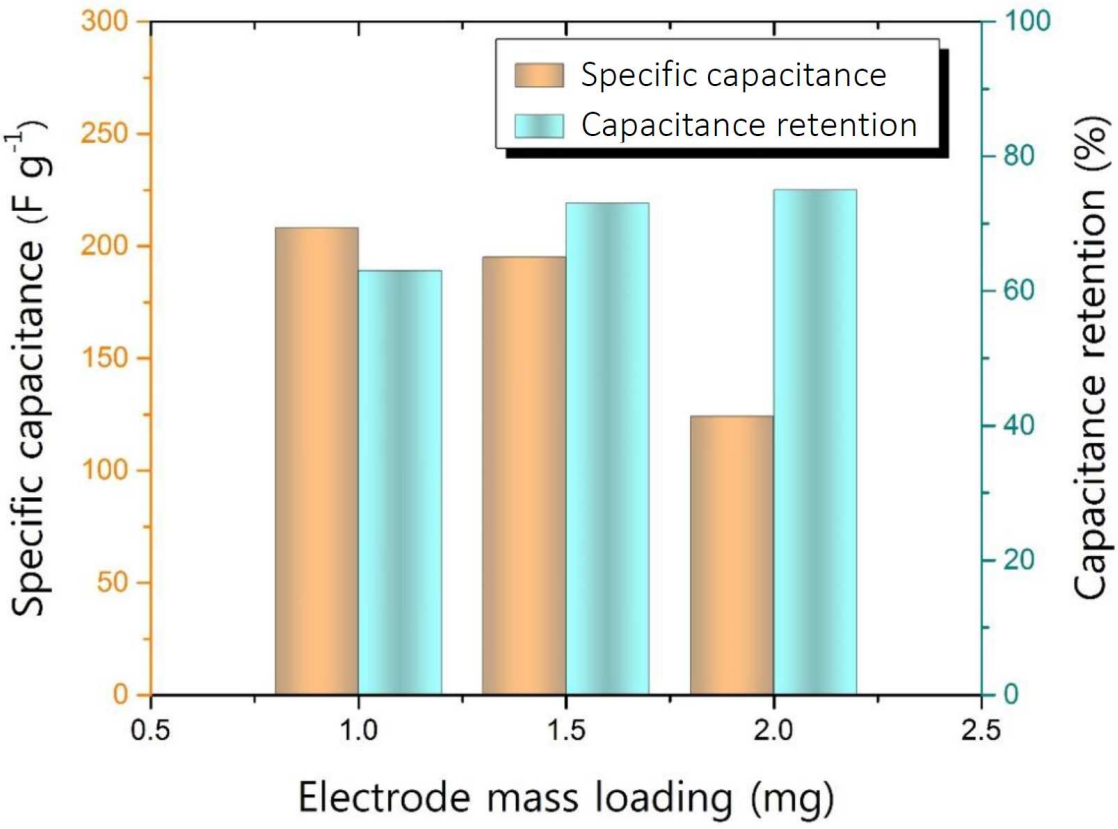

Figure 4 | Dependence of specific capacitance on different mass loadings at a scan rate of 20 $mV \cdot s^{-1}$, and dependence of capacitance retention on mass loading at a scan rate of 200 $mV \cdot s^{-1}$.

Figure 5

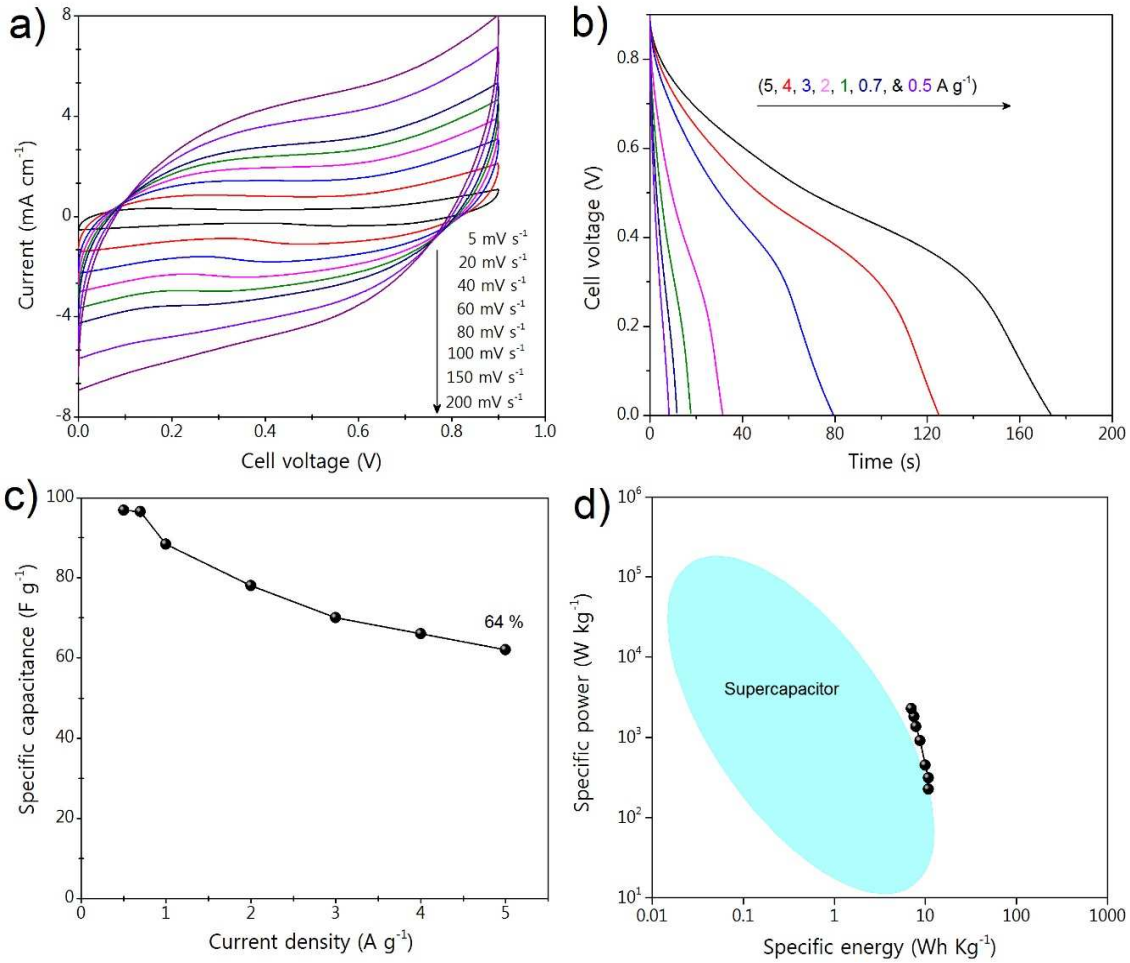

Figure 5 | (a) CV curves of symmetric cell based on large-sized NPC at different scan rates, (b) galvanostatic-discharge curves at various current densities in the potential range from 0 to 0.9 V, (c) specific capacitance at different current densities in the range of 0.5 to 5 A·g^{-1}, and (d) Ragone plot for symmetric supercapacitor based on large-sized NPC at different scan rates.

Figure 6

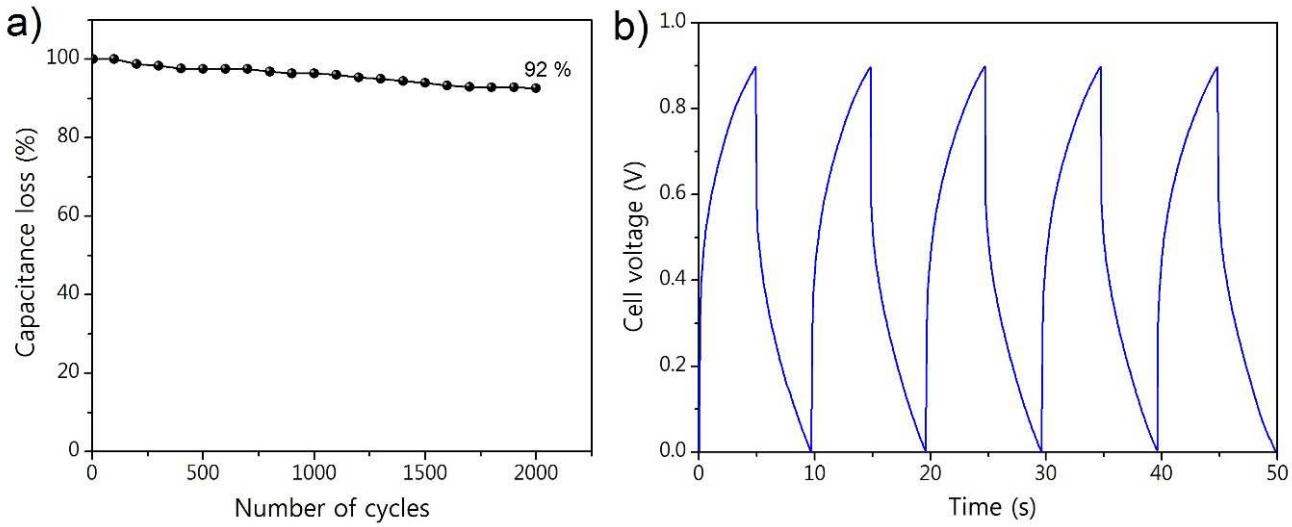

Figure 6 | (a) Cycling performance of symmetric cell based on large-sized NPC at current density of 7.5 $A \cdot g^{-1}$; and (b) arbitrarily chosen charge-discharge cycles, showing the good stability of the cell.

A Table of Contents

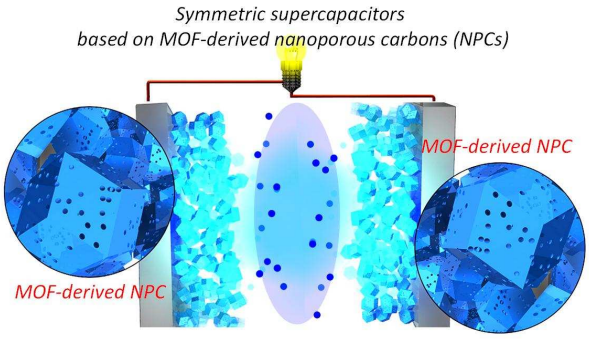

We design novel symmetric supercapacitors based on nanoporous carbons (NPCs) by direct carbonization of Zn-based metal organic frameworks (MOFs).